Journal of Quantitative Spectroscopy & Radiative Transfer 256 (2020) 107303

Contents lists available at ScienceDirect

Journal of Quantitative Spectroscopy & Radiative Transfer

journal homepage: www.elsevier.com/locate/jqsrt

MRCI+Q study on the electronic structure and spectroscopy of the low-lying electronic states of HgBr including spin-orbit coupling

Shutao Zhao[a,b,**], Jicheng Cui[b], Rui Li[c], Cunhua Zhang[c], Bing Yan[d,*]

[a] Key Laboratory of Functional Materials and Devices for Informatics of Anhui Higher Education Institutes, School of Physics and Electronic Science, Fuyang Normal University, Fuyang 236037, China
[b] Changchun Institute of Optics, Fine Mechanics and Physics, Chinese Academy of Sciences, Changchun 130033, China
[c] Department of Physics, College of Science, Qiqihar University, Qiqihar 161006, China
[d] Institute of Atomic and Molecular Physics, Jilin University, Changchun 130012, China

ARTICLE INFO

Article history:
Received 1 June 2020
Revised 28 August 2020
Accepted 30 August 2020
Available online 31 August 2020

Keywords:
HgBr
Configuration interaction
Spin-orbit coupling
Spectroscopic constant
Potential energy curve

ABSTRACT

Due to attractive candidate for the laser application and searching for the permanent electric dipole moment of the electron (eEDM), mercury bromide (HgBr) is of much interest to researchers. However, detailed information of the electronic structure of HgBr is still lacking, especially for spin-orbit interactions in excited states. In this work, high-level configuration interaction calculations of low-lying states correlating to the lowest two dissociation limits Hg(^{1}S) + Br(^{2}P) and Hg(^{3}P) + Br(^{2}P) of HgBr are carried out. In order to ensure good accuracy, the Davidson correction and spin-orbit coupling (SOC) effect are all taken into consideration in our computations. The potential energy curves (PECs) of 14 Λ-S states and 30 Ω states are determined. Based on the PECs, the spectroscopic constants of the bound states are obtained, most of which have not been reported in previous studies. The calculated SOC integrals of $2^2\Sigma^+$-$2^2\Pi$ indicate a strong spin-orbit interaction, which can explain the apparent perturbations between $B^2\Sigma^+_{1/2}$ and $C^2\Pi_{1/2}$ found in the HgBr fluorescence excitation spectrum. Finally, to reveal more detail on transition properties of excited states, transition dipole moments of $C^2\Pi_{1/2}$-$X^2\Sigma^+_{1/2}$, $D^2\Pi_{3/2}$-$X^2\Sigma^+_{1/2}$, and $B^2\Sigma^+_{1/2}$-$X^2\Sigma^+_{1/2}$ transitions and radiative lifetimes of $C^2\Pi_{1/2}$, $D^2\Pi_{3/2}$, and $B^2\Sigma^+_{1/2}$ are determined.

1. Introduction

Due to the important role of mercury halides in chemical reactions and environmental science [1,2], much efforts have been made to understand how mercury species are introduced into the environment. The gas phase HgBr molecule, a basic mercury specimen, is of particular interest being the initial oxidation step of atmospheric Hg via Hg + Br, which is important in mercury depletion events [3,4]. As the observation of lasing in the visible spectral region has been reported in the reaction $HgBr(B^2\Sigma^+) \rightarrow HgBr(X^2\Sigma^+) + h\nu$, HgBr dissociation laser also has gained a lot of attention [5–7]. Another motivation for investigating the electronic structure of HgBr is to seek molecular candidates for permanent electric dipole moment of the electron (eEDM) searches [8]. Mercury monohalides are heavy polar diatomic molecules, which are possible primary tools for eEDM searching experiments. Thus, detailed electronic structure information of low-lying electronic states of HgBr is valuable to aid such research.

Experimentally, pioneering analysis on the characteristic bands of HgBr in the Nitrogen after-glow was carried out by Wieland in 1929 [9], where three classes of bands (2450–2700 Å, 2650–2900 Å and 3200–5000 Å) were categorized. The Class I (2450–2700 Å) and II (2650–2900 Å) bands degraded to violet, which were ascribed to the diatomic molecule HgBr and the triatomic molecule $HgBr_2$, respectively. The Class III bands occurring in the longer region (3200–5000 Å) were diffuse and complex. Since then, many spectral experiments have been performed on ground and lower excited states of HgBr. For Class II bands (2650–2900 Å), Sastri ascribed the ultraviolet bands to the $^2\Sigma$–$^2\Sigma$ transition in HgBr [10]. Howell analyzed the strongest groups of heads at 34,580 and 34,668 cm^{-1} and concluded they were Δ = 0 sequences of the $^2\Pi$–$^2\Sigma$ transition [11]. Rao found a new headless and

* Corresponding author.
** Corresponding author at: Key Laboratory of Functional Materials and Devices for Informatics of Anhui Higher Education Institutes, School of Physics and Electronic Science, Fuyang Normal University, Fuyang 236037, Chin.
E-mail addresses: zhaoshutao2002@163.com (S. Zhao), yanbing@jlu.edu.cn (B. Yan).

https://doi.org/10.1016/j.jqsrt.2020.107303
0022-4073/

diffuse band system in the ultraviolet region between 2430 and 2470 Å, which was assigned to the $^2\Sigma$-$X^2\Sigma$ transition [12]. Krishnamurthy [13] photographed the ultraviolet bands in the region of 2720–2900 Å and then divided the bands lying in 2770–2900 Å into two systems arising from the two components of $^2\Pi$–$^2\Sigma$ transition with a separation of $^2\Pi$ equal to 3828 cm^{-1}, while another system lying between 2720 and 2770 Å was probably due to a $^2\Sigma$–$^2\Sigma$ transition. Later, Greig[14] obtained the spectroscopic constants T_e = 34,741 cm^{-1}, and ω_e' = 274 cm^{-1} of $C(2)^2\Pi_{1/2}$ by analyzing $C(2)^2\Pi_{1/2}$-$X^2\Sigma^+{}_{1/2}$ bands in absorption spectroscopy. Misra et al. [15] observed the emission bands of $C(2)^2\Pi_{1/2}$-$X^2\Sigma^+{}_{1/2}$ (2730–2940 Å) and $D(2)^2\Pi_{3/2}$-$X^2\Sigma^+{}_{1/2}$ (2471–2665 Å) systems of HgBr radical in the collision experiments of N^+ and N_2^+ with $HgBr_2$ molecules, which both degraded to red. Schimitschek et al. [5] measured the laser spectra of the $B(2)^2\Sigma^+{}_{1/2} \rightarrow X^2\Sigma^+{}_{1/2}$ band using an ArF excimer laser photodissociation of $HgBr_2$, whose wavelengths range from 502 to 505 nm. The radiative lifetime of the vibrational level v'=0 of $B(2)^2\Sigma^+{}_{1/2}$ was measured to be 23.3 ns [16]. Tellinghuisen et al. [17] analyzed the $B(2)^2\Sigma^+{}_{1/2} \rightarrow X^2\Sigma^+{}_{1/2}$ emission spectrum of HgBr and gave an estimate of the dissociation energy D_e = 0.6819 eV lower than that of Wieland's earlier analysis for ground state $X^2\Sigma^+{}_{1/2}$. They also evaluated the spectroscopic constants of $B(2)^2\Sigma^+{}_{1/2}$ and $X^2\Sigma^+{}_{1/2}$. These experimental studies mainly concentrated on low-lying states, such as ground state $X^2\Sigma^+{}_{1/2}$ and excited state $B^2\Sigma^+{}_{1/2}$ et al., but the spectral properties of other states remain unclear or inadequate.

Although there have been a number of experiments on the low-lying states of HgBr, few theoretical studies on its electronic structure have been performed. Wadt [18] obtained the equilibrium distance R_e for $X^2\Sigma^+$ and $B(2)^2\Sigma^+$using the configuration interaction (CI) method, and also gave an estimated value (27.6 ns) of the radiative lifetime for the $B(2)^2\Sigma^+$ state. Bhartiya et al. [19] determined the dissociation energy D_e = 0.64 eV for the $X^2\Sigma^+$state by fitting empirical potential functions. Later, Liao et al. predicted the equilibrium distance R_e and harmonic vibrational frequency ω_e of $X^2\Sigma^+$ with the relativistic density-functional method [20]. In 2005, Shepler et al. performed accurate calculations on the D_e, R_e, and ω_e of the ground state $X^2\Sigma^+{}_{1/2}$ via a composite approach up to full quadruple excitations [3]. In order to search for attractive candidates in future eEDM experiments, Prasannaa et al. performed accurate relativistic coupled cluster calculations of the effective electric fields on mercury monohalides[8]. All the above theoretical studies mainly concentrated on the ground state. However, for higher excited states of HgBr molecule detected but not characterized in previous experimental work, theoretical investigations are still lacking.

In this work, high-level computational investigations have been carried out on low-lying states of the HgBr molecule. In order to accurately estimate spectroscopic constants, the electrons correlations of the 5d shell of Hg, spin-orbit coupling (SOC) effect and the Davidson's correction are all taken into consideration in our calculations, which exhibit significant influence on the electronic structures and dissociation energies [21,22]. The potential energy curves (PECs) of the 14 Λ-S states correlating to the lowest two asymptotes of HgBr, as well as the 30 Ω states associated with the lowest eight asymptotes are calculated. Based on the calculated PECs, the spectroscopic constants of low-lying bound states are obtained. With the aid of SO matrix elements, the perturbations on the $C^2\Pi_{1/2}$ states are analyzed in detail. Finally, the radiative lifetimes of the six low-lying vibrational levels of $B^2\Sigma^+{}_{1/2}$, $C^2\Pi_{1/2}$ and $D^2\Pi_{3/2}$ states are derived. Our present work reports a high-level computational study on low-lying electronic states of HgBr, which can provide helpful information for these states.

2. Methods

High-level *ab initio* calculations on HgBr are performed with the help of the MOLPRO 2012 software package [23]. C_{2v} symmetry is employed in our calculations, and the relationships for the irreducible representations of C_{2v} and $C_{\infty v}$ are as follows: $\Sigma^+ = A_1$, $\Pi = B_1 + B_2$, $\Delta = A_1 + A_2$ and $\Sigma^- = A_2$. For the basis sets of HgBr, cc-pwCV5Z-PP [24] with ECP60MDF [25] and cc-pwCV5Z-PP [26] with ECP10MDF [27] are selected for Hg and Br, respectively. For a series of HgBr bonds (with step sizes of 0.05 Å for R = 1.9–4.0, 0.1 Å for R = 4.0–6.0, and 0.5 Å for R = 6.0–10.0), the single-configuration wavefunction of the ground state is calculated with the Hartree–Fock (HF) method. Utilizing the HF molecular orbitals as the starting orbitals, state-averaged complete active space self-consistent field (SA-CASSCF) calculations for 14 Λ-S states are performed to generate multi-configuration wavefunctions [28,29]. The 14 Λ-S states are the ground state $X^2\Sigma^+$, $1^2\Pi$ correlating with the lowest asymptote $Hg(^1S) + Br(^2P)$, and 12 other molecular states ($2^2\Sigma^+$, $3^2\Sigma^+$, $2^2\Pi$, $3^2\Pi$, $1^2\Delta$, $1^2\Sigma^-$, $1^4\Sigma^+$, $2^4\Sigma^+$, $1^4\Delta$, $1^4\Sigma^-$, $1^4\Pi$, $2^4\Pi$) correlating with the second asymptote $Hg(^3P) + Br(^2P)$. Finally, the internally contracted multi-reference configuration interaction including Davidson correction (icMRCI+Q) [30,31] calculations are carried out to consider the dynamical correlation and size-consistency error for the 14 Λ-S states of the HgBr molecule. In the above CASSCF calculations, seven molecular orbitals (MOs) and seven electrons are chosen in the active space, which include three A_1, two B_1 and two B_2, corresponding to the 6s6p shells of the Hg atom as well as 4p shells of the Br atom. In the icMRCI+Q calculations, the $5d^{10}$ electrons of Hg and $4s^2$ electrons of Br are placed into the close shell. The electrons in close shell are correlated through single and double excitations. Thus, there are a total of 19 electrons in the correlation energy computations. The inner electrons correlated with 5s5p shells of Hg and 3s3p3d shells of Br are kept frozen and not correlated. The SOC effect is considered via a state-interacting approach with the ECP spin-orbit operator using a two-step perturbative procedure [32–34]. Finally, the energies of Ω states are determined by the diagonalization of the calculated SO matrix.

Based on the calculated PECs of the Λ-S and Ω states, spectroscopic constants of bound states are determined by the solution of the Schrödinger equation with the help of the LEVEL procedure [35]. The transition probabilities of $C^2\Pi$, $B^2\Sigma^+$, $C^2\Pi_{1/2}$, $D^2\Pi_{3/2}$ and $B^2\Sigma^+{}_{1/2}$ are then calculated, and the radiative lifetimes of the low vibrational levels of $C^2\Pi_{1/2}$, $D^2\Pi_{3/2}$ and $B^2\Sigma^+{}_{1/2}$ are estimated.

3. Results and discussion

3.1. PECs of Λ-S states

The spin-free PECs of 14 Λ-S states of HgBr correlating to the asymptotes $Hg(^1S) + Br(^2P)$ and $Hg(^3P) + Br(^2P)$ are calculated by the MRCI+Q method and shown in Fig. 1. The energy difference between the asymptotes $Hg(^1S) + Br(^2P)$ and $Hg(^3P) + Br(^2P)$ is 41,150 cm^{-1}, in good agreement with the experimental value 41,788 cm^{-1}. [36] Among the Λ-S states shown in Fig. 1, the states $X^2\Sigma^+$, $B^2\Sigma^+$, $C^2\Pi$, $3^2\Sigma^+$, $1^2\Delta$, $1^2\Sigma^-$, $1^4\Sigma^+$, $1^4\Sigma^-$ and $1^4\Delta$ are bound, whose spectroscopic constants are shown in Table 1.

As presented in Table 1, the ground state of the HgBr molecule is $X^2\Sigma^+$, arising from the electronic configuration $8\sigma^2 9\sigma^\alpha 5\pi^4(81)$. Considering the correlation of $5d^{10}$ electrons of Hg and $4s^2$ electrons of Br in the MRCI+Q calculation, the ω_e and $\omega_e x_e$ of $X^2\Sigma^+$are calculated to be 178.26 and 0.98 cm^{-1}, respectively, differing slightly from experimental results (186.47 and 0.97 cm^{-1}) [37] by 8.21 and 0.01 cm^{-1}. As far as we know, the previous theoretical values of R_e are in the range of 2.49–2.61 Å [3,4,18–20]. The

Table 1
Spectroscopic constants of Λ-S states of HgBr.

state		T_e (cm^{-1})	ω_e (cm^{-1})	$\omega_e x_e$ (cm^{-1})	B_e (cm^{-1})	R_e (Å)	D_e (eV)	Configuration at R_e(%)
$X^2\Sigma^+$	This work	0	178.26	0.98	0.0459	2.5337	0.7036	$8\sigma^2 9\sigma^\alpha 5\pi^4$(81)
	Expt.[a]	0	186.47	0.97			0.7117	
	Expt.[b]	0	188.25	1.04	0.0435		0.6819	
	Expt.[c]	0	186.77					
	Expt.[d]	0					0.54±0.20	
	Calc.[e]	0	159.4	1.64	0.044	2.61	0.48	
	Calc.[f]	0					0.64	
	Calc.[g]	0	176			2.60		
	Calc.[h]	0	192.7			2.4976	0.7190	
	Calc.[i]	0	193.8	0.98		2.494	0.6956	
$B^2\Sigma^+$	This work	23,609	141.57	0.23	0.0316	3.056	2.8743	$8\sigma^2 9\sigma^\alpha 5\pi^4$(29) $8\sigma^\alpha 9\sigma^2 5\pi^4$(44)
	Expt.[a]	23,485	135.08	0.28			2.4710	
	Expt.[b]	23,485	135.89	0.25	0.0293			
	Expt.[j]	23,485	135.08	0.28				
	Expt.[k]	23,489	135.95	0.25				
	Calc.[e]	21,778	141.8	0.29	0.032	3.04	4.77	
$C^2\Pi$	This work	36,581	223.05	0.82	0.0500	2.4285	1.2697	$8\sigma^2 5\pi^4 6\pi^\alpha$(77)
	Expt.[j]	37,611	241.03	1.17				
$3^2\Sigma^+$	This work	46,398	26.88	0.48	0.0240	3.5084	0.0512	$8\sigma^2 9\sigma^\alpha 5\pi^{\alpha\beta\beta} 6\pi^\alpha$(63) $8\sigma^2 9\sigma^\alpha 5\pi^{\alpha\alpha\beta} 6\pi^\beta$(20)
$1^2\Delta$	This work	45,833	50.46	0.71	0.0292	3.1780	0.1201	$8\sigma^2 9\sigma^\alpha 5\pi^{\alpha\beta\beta} 6\pi^\alpha$(86) $8\sigma^2 9\sigma^\alpha 5\pi^{\alpha\alpha\beta} 6\pi^\beta$(13)
$1^2\Sigma^-$	This work	46,113	44.29	0.74	0.0282	3.2355	0.0857	$8\sigma^2 9\sigma^\alpha 5\pi^{\alpha\beta\beta} 6\pi^\alpha$(86) $8\sigma^2 9\sigma^\alpha 5\pi^{\alpha\alpha\beta} 6\pi^\beta$(13)
$1^4\Sigma^+$	This work	44,496	83.78	0.86	0.0346	2.9197	0.2873	$8\sigma^2 9\sigma^\alpha 5\pi^{\alpha\alpha\beta} 6\pi^\alpha$(98)
$1^4\Sigma^-$	This work	45,720	61.87	0.93	0.0314	3.0646	0.1350	$8\sigma^2 9\sigma^\alpha 5\pi^{\alpha\alpha\beta} 6\pi^\alpha$(99)
$1^4\Delta$	This work	45,183	73.31	0.90	0.0331	2.9854	0.2025	$8\sigma^2 9\sigma^\alpha 5\pi^{\alpha\alpha\beta} 6\pi^\alpha$(99)

[a] Ref. [37].
[b] Ref. [17].
[c] Ref. [49].
[d] Ref. [46].
[e] Ref. [18].
[f] Ref. [19].
[g] Ref. [20].
[h] Ref. [3].
[i] Ref. [4].
[j] Ref. [47].
[k] Ref. [48].

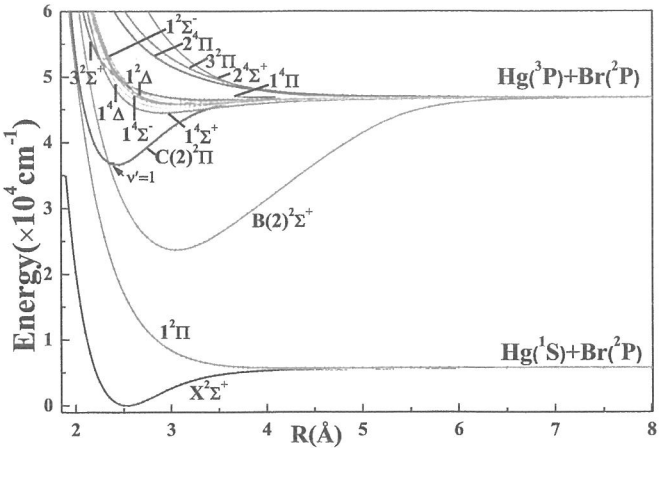

Fig. 1. Potential energy curves of 14 Λ-S states of HgBr correlating to the lowest two asymptotes Hg(^{1}S) + Br(^{2}P) and Hg(^{3}P) + Br(^{2}P).

MRCI method used in our calculations does not consider size-consistency, so the Davidson correction (+Q) is added to balance related error. The coupled cluster calculations with iterative triple and quadruple (CCSDTQ) excitations adopted in Shepler and Peterson's work [3] are size-consistent. The spectroscopic constant of the $X^2\Sigma^+$ obtained by reference [3] is more reliable, which can be regarded as the benchmark. The R_e and D_e in our work is computed to be 2.5337 Å and 0.7036 eV, which is in good agreement with the accurate theoretical value of 2.4976 Å and 0.7190 eV. The deviation between our computation and reference [3] may originate from the correlation effect of electron. After considering the effect of SOC, the relatively large deviation of D_e for $X^2\Sigma^+$is expected to be reduced, which will be discussed later. The first excited state $1^2\Pi$ correlates to the lowest dissociation limit Hg(^{1}S)+Br(^{2}P), whose vertical excitation energy is 15,541 cm^{-1}.

The B(2) $^2\Sigma^+$ state originating from the electronic configurations $8\sigma^2 9\sigma^\alpha 5\pi^4$ (29%) and $8\sigma^\alpha 9\sigma^2 5\pi^4$ (44%) indicates its multi-configurational properties. When considering the correlated effect our calculate values for spectroscopic constants T_e, ω_e, $\omega_e\chi_e$, and B_e are 23,609, 141.57, 0.23, and 0.0316 cm^{-1}, close to the experimental values from the $B^2\Sigma^+$-$X^2\Sigma^+$ emission spectrum of HgBr [17]. For equilibrium distance R_e, our calculated value of 3.056 Å is close to the only theoretical result of 3.04 Å estimated by Wadt [18]. However, for dissociation energy D_e, the difference between our prediction and Wadt's theoretical result is as large as ~1.9 eV. In comparison to the available experimental D_e (2.4710 eV), our calculated value is about 0.4 eV overestimated. The SO effect is important for the D_e of the HgBr molecule containing high-Z elements, which will be discussed in the next section.

The main configuration of $C(2)^2\Pi$ is $8\sigma^2 5\pi^4 6\pi^\alpha$ (77%), corresponding to the $9\sigma \rightarrow 6\pi$ transition. The potential well depth of the $C^2\Pi$ state is predicated to be 1.2697 eV, which implies a large binding energy, similar to that of the B(2) $^2\Sigma^+$ state. As depicted in Fig. 1, $C(2)^2\Pi$ and B(2) $^2\Sigma^+$ cross with each other at the region $R = 2.35$ Å, which can cause perturbations to these two bound states.

Table 2
Dissociation asymptotes of the low-lying Ω states of HgBr.

Atomic state (Hg +Br)	Ω state	energy(cm^{-1})	
		this work	Expt.[a]
$^1S_0+^2P_{3/2}$	3/2,1/2	0	0
$^1S_0+^2P_{1/2}$	1/2	3528	3685
$^3P_0+^2P_{3/2}$	3/2,1/2	37,365	37,645
$^3P_1+^2P_{3/2}$	5/2, 3/2, 3/2,1/2, 1/2, 1/2,	39,262	39,412
$^3P_0+^2P_{1/2}$	1/2	40,885	41,330
$^3P_1+^2P_{1/2}$	3/2,1/2, 1/2	42,782	43,098
$^3P_2+^2P_{3/2}$	7/2,5/2, 5/2,3/2, 3/2, 3/2, 1/2, 1/2, 1/2,1/2	43,054	44,043
$^3P_2+^2P_{1/2}$	5/2,3/2, 3/2, 1/2, 1/2	46,578	47,728

[a] Ref. [36].

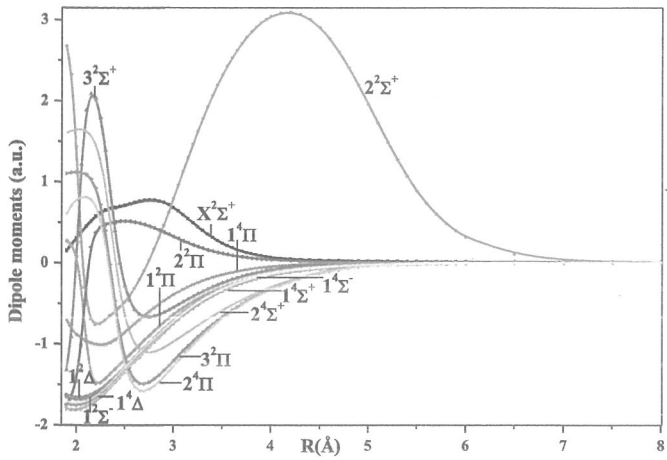

Fig. 2. Dipole moments of 14 Λ-S states of HgBr.

The dipole moments (DMs) of spin-free Λ-S states correlating to the asymptotes Hg(^{1}S) + Br(^{2}P) and Hg(^{3}P) + Br(^{2}P) are also calculated at MRCI level in this paper, as displayed in Fig. 2. To clarify values of the DMs, the sign convention is defined so that positive corresponds to the Hg^+Br^-polarity. According to this sign convention, the DM of $X^2\Sigma^+$at the equilibrium distance R_e = 2.55 Å is computed to be 0.73 a.u., indicating the ionic bonding nature of $Hg^{\delta+}Br^{\delta-}$. Our obtained DM value of $X^2\Sigma^+$for HgBr molecule is quantitatively consistent with that of the isovalent molecule CdBr (1.00 a.u.) [38]. All DMs of these spin-free Λ-S states tend to zero for a large distance R > 8 Å, which corresponds with the covalent dissociation limit.

3.2. PECs of the Ω states

The spin-orbit effects are considered via a two-step perturbation procedure as successfully utilized in previous theoretical papers [39,40]. Previous investigations reveal that the SOC is of great importance to spectroscopic properties of molecules including high-Z elements [41–45]. When considering the SOC for the heavy metal bromide HgBr molecule, a given multiplet Λ-S state can split into several different Ω states. Therefore, there are 30 Ω states in total generated from the 14 Λ-S states of the HgBr molecule. All PECs of the 30 Ω states are calculated, however for the sake of visual clarity the PECs of high-

Table 3
Spectroscopic constants of the Ω states of HgBr.

state		T_e(cm^{-1})	ω_e(cm^{-1})	$\omega_e x_e$(cm^{-1})	B_e(cm^{-1})	R_e(Å)	D_e(eV)	Dominant Λ-S composition at respective R_e (%)
$X^2\Sigma^+{}_{1/2}$	This work	0	176.46	1.05	0.0459	2.5351	0.5763	$X^2\Sigma^+$(99.48)
	Expt.[a]	0	186.47	0.97			0.7117	
	Expt.[b]	0	188.25	1.04	0.0435		0.6819	
	Expt.[c]	0	186.77					
	Expt.[d]	0					0.54±0.20	
	Calc.[e]	0	159.4	1.64	0.044	2.61	0.48	
	Calc.[f]	0					0.64	
	Calc.[g]	0	192.7			2.4976	0.7190	
	Calc.[h]	0	193.8	0.98		2.494	0.6956	
	Calc.[i]	0	176			2.60		
$B^2\Sigma^+{}_{1/2}$	This work	23,569	140.93	0.23	0.0314	3.0623	2.2858	$2^2\Sigma^+$(98.73)
	Expt.[a]	23,485	135.08	0.28			2.4710	
	Expt.[b]	23,485	135.89	0.25	0.0293			
	Expt.[j]	23,485	135.08	0.28				
	Expt.[k]	23,489	135.95	0.25				
	Calc.[e]	21,778	141.8	0.29	0.032	3.04	4.77	
$C^2\Pi_{1/2}$	This work	35,001	282.41	1.76	0.0492	2.4352		$2^2\Pi$(94.56)
	Expt.[c]	34,719	278.67	1.84	0.0452			
	Expt.[j]	34,722	278.63	1.82				
$D^2\Pi_{3/2}$	This work	38,455	216.14	1.00	0.0497	2.4358		$2^2\Pi$(99.44)
	Expt.[c]	38,573	228.46	0.87	0.0465			
	Expt.[k]	38,573	231.23	0.99				
	Expt.[l]	38,574	228.5	0.95				

[a] Ref. [37].
[b] Ref. [17].
[c] Ref. [49].
[d] Ref. [46].
[e] Ref. [18].
[f] Ref. [19].
[g] Ref. [3].
[h] Ref. [4].
[i] Ref. [20].
[j] Ref. [47].
[k] Ref. [48].
[l] Ref. [56].

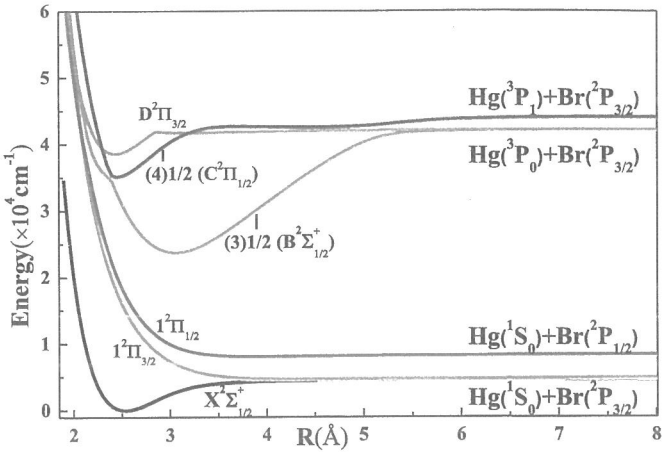

Fig. 3. Potential energy curves of low-lying Ω states of HgBr.

Table 4
Oscillator strength f and vertical excitation energies of the low-lying excited states.

Electronic states	oscillator strength f (a.u.) at R_e	vertical excitation energies (cm^{-1})
$1^2\Pi_{3/2}$	0.001	14,428
$1^2\Pi_{1/2}$	0.003	16,844
$B^2\Sigma^+{}_{1/2}$	0.043	29,489
$C^2\Pi_{1/2}$	0.057	35,424
$D^2\Pi_{3/2}$	0.064	38,878

lying repulsive states are not presented. Fig. 3 shows the PECs of six low-lying Ω states of HgBr, including four bound states ($X^2\Sigma^+{}_{1/2}$, $B(2)^2\Sigma^+{}_{1/2}$, $C(2)^2\Pi_{1/2}$ and $D(2)^2\Pi_{3/2}$) and two repulsive states ($1^2\Pi_{1/2}$ and $1^2\Pi_{3/2}$). The dissociation relationship for the Ω states is shown in Table 2. Eight asymptotes $Hg(^1S_0) + Br(^2P_{3/2})$, $Hg(^1S_0) + Br(^2P_{1/2})$, $Hg(^3P_0) + Br(^2P_{3/2})$, $Hg(^3P_0) + Br(^2P_{1/2})$, $Hg(^3P_1) + Br(^2P_{3/2})$, $Hg(^3P_1) + Br(^2P_{1/2})$, $Hg(^3P_2) + Br(^2P_{3/2})$, and $Hg(^3P_2) + Br(^2P_{1/2})$ are generated from the asymptotes $Hg(^1S) + Br(^2P)$ and $Hg(^3P) + Br(^2P)$. The calculated energy separations of $Hg(^1S_0) + Br(^2P_{1/2})$, $Hg(^3P_0) + Br(^2P_{3/2})$, $Hg(^3P_1) + Br(^2P_{3/2})$, $Hg(^3P_0) + Br(^2P_{1/2})$, $Hg(^3P_1) + Br(^2P_{1/2})$, $Hg(^3P_2) + Br(^2P_{3/2})$, and $Hg(^3P_2) + Br(^2P_{1/2})$ with respect to the first dissociation asymptote $Hg(^1S_0) + Br(^2P_{3/2})$ are 3528, 37,365, 39,262, 40,885, 42,782, 43,054 and 46,578 cm^{-1}, respectively, differing from corresponding experimental values [36] by 157, 280, 150, 445, 316, 989 and 1150 cm^{-1}, showing a reasonable accordance.

The spectroscopic constants of the four low-lying bound Ω states and their leading Λ-S compositions at R_e are shown in Table 3. Table 4 presents the vertical excitation energies and oscillator strength f of the low-lying Ω states. Since $X^2\Sigma^+{}_{1/2}$ is mainly composed of $X^2\Sigma^+$ (99.48%), the spectroscopic constants are almost unchanged. However, due to the SOC effect, the D_e of $X^2\Sigma^+{}_{1/2}$ is 0.5763 eV, which is 0.1273 eV lower than that of $X^2\Sigma^+$ (0.7036 eV) at MRCI+Q level. For the ground state $X^2\Sigma^+{}_{1/2}$, the experimental values of D_e are fairly disparate (0.7117 eV, 0.6819 eV, and 0.54 ± 0.20 eV) [17,37,46]. Our present theoretical value of 0.5763 eV lies within this experimental range. The excited states $1^2\Pi_{1/2}$ and $1^2\Pi_{3/2}$ generated from the first excited state $1^2\Pi$ correlate with different asymptotes $Hg(^1S_0) + Br(^2P_{1/2})$ and $Hg(^1S_0) + Br(^2P_{3/2})$, respectively. The vertical excitation energies and oscillator strength of $1^2\Pi_{1/2}$ and $1^2\Pi_{3/2}$ are 16,844 cm^{-1}, 0.003 and 14,428 cm^{-1}, 0.001, respectively. The weak oscillator

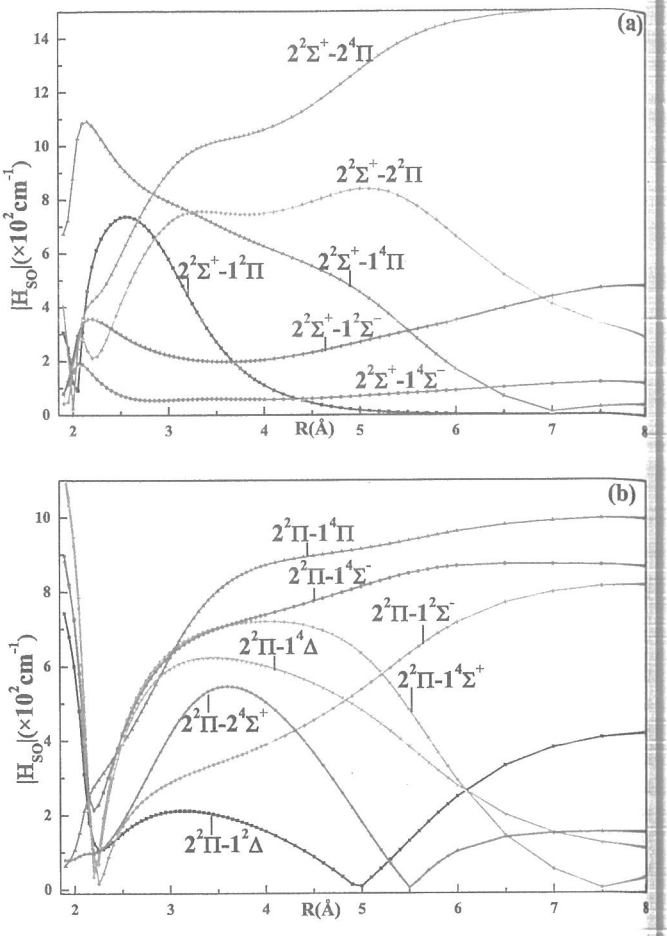

Fig. 4. Evolution of spin-orbit matrix elements related to $2^2\Sigma^+$ and $2^2\Pi$ of HgBr. (See Table S1 for the definition of these spin-orbit matrix elements.).

strengths of $1^2\Pi_{1/2}$ and $1^2\Pi_{3/2}$ indicate difficulty in detecting the absorption spectra of $1^2\Pi_i$-$X^2\Sigma^+{}_{1/2}$ transitions.

Once the SOC effect is considered, the $2^2\Pi$ splits into two Ω states $C(2)^2\Pi_{1/2}$ and $D(2)^2\Pi_{3/2}$, while $B(2)\ ^2\Sigma^+$ corresponds to one Ω state $B(2)^2\Sigma^+{}_{1/2}$. Because of the avoided crossing, $C(2)^2\Pi_{1/2}$ and $B(2)^2\Sigma^+{}_{1/2}$ have a common Ω= 1/2 component and will recombine into new excited states Ω = (3)1/2 and Ω = (4)1/2, as shown in Fig. 3. For $R \geq 2.4$ Å, the PECs of (3)1/2 and (4)1/2 originate from $B(2)^2\Sigma^+{}_{1/2}$ and $C(2)^2\Pi_{1/2}$, respectively. Some experimental data exists [17,37,47,48] for T_e, ω_e and $\omega_e x_e$ of $B(2)^2\Sigma^+{}_{1/2}$ listed in Table 3. Our calculated values of T_e, ω_e and $\omega_e x_e$ are 23,569, 140.93, and 0.23 cm^{-1}, respectively, which are close to the available experimental values [47,49]. For the spectroscopic constant B_e, our theoretical value 0.0314 cm^{-1} is in good agreement with the experimental value [17] 0.0293 cm^{-1} and theoretical value [18] 0.032 cm^{-1}. For the D_e of $B(2)^2\Sigma^+{}_{1/2}$, only one experimental value 2.4710 eV has been reported [37]. When considering the SO effect, the calculated D_e of $B(2)^2\Sigma^+{}_{1/2}$ is 2.2858 eV, showing better agreement with the experimental value than that of the pure Λ-S state $B(2)^2\Sigma^+$. The calculated R_e of $B(2)^2\Sigma^+{}_{1/2}$ (3.0623 Å) is obviously bigger than that of $X^2\Sigma^+{}_{1/2}$ (2.5351 Å) which gives rise to the long vibrational progression B → X located in (0-ν″) (ν″ = 16–20) bands. Our present results are in good agreement with experimental observations of (0-ν″) (ν″ = 17–22) transitions in the B → X emission bands of HgBr [50]. The calculated R_e of $B(2)^2\Sigma^+{}_{1/2}$ is 0.5272 Å larger than that of $X^2\Sigma^+{}_{1/2}$ agreeing well with the experimental result 0.57 Å [17]. The T_e

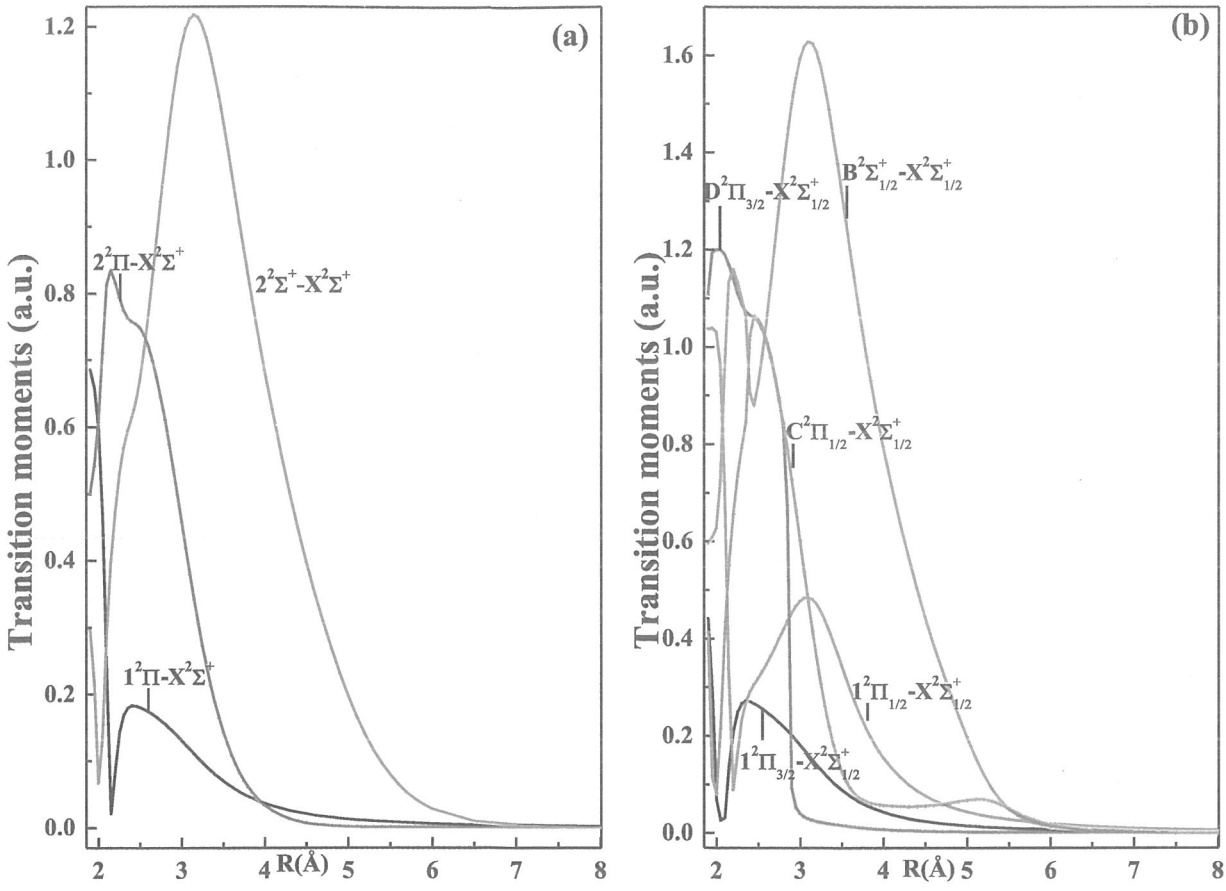

Fig. 5. Transition dipole moments of $2^2\Sigma^+$-$X^2\Sigma^+$, $1^2\Pi$-$X^2\Sigma^+$and $2^2\Pi$-$X^2\Sigma^+$ (a) excluding and (b) including SOC effect.

ω_e and $\omega_e x_e$ of $C(2)^2\Pi_{1/2}$ are calculated to be 35,001, 282.41 and 1.76 cm^{-1}, which are all in good agreement with the previous experimental values 34,722, 278.63, and 1.82 cm^{-1}, respectively [47]. The B_e of $C(2)^2\Pi_{1/2}$ is calculated to be 0.0492 cm^{-1}, only 0.004 cm^{-1} larger than the experimental result [49]. For the T_e, ω_e, and $\omega_e x_e$ of $D(2)^2\Pi_{3/2}$, our calculated results are 38,455, 216.14 and 1.00 cm^{-1}, differing from the experimental value [48] only by 118 (0.3%), 15.09 (6.5%) and 0.01 cm^{-1} (1.0%), respectively. B_e is calculated to be 0.0497 cm^{-1}, only 0.0032 cm^{-1} larger than the experimental value [49]. Our calculated energy separation of $C(2)^2\Pi_{1/2}$-$D(2)^2\Pi_{3/2}$ is 3454 cm^{-1}, which is reasonably close to the experimental value of 3906 [11], 3833 [14], and 3828 cm^{-1} [13]. The calculated oscillator strengths f of $B(2)^2\Sigma^+{}_{1/2}$, $C(2)^2\Pi_{1/2}$, and $D(2)^2\Pi_{3/2}$ states are 0.043, 0.057, and 0.064, respectively, which are large enough to form strong spectra bands [15,51].

3.3. Spin-orbit coupling and predissociation

The absolute values of SOC integrals involving the low excited states $2^2\Sigma^+$ and $2^2\Pi$ are determined to quantitatively estimate the SO interactions, which are shown in Fig. 4. The definitions of the schematic representation for the SO matrix elements are listed in Table S1 (Supplementary Materials). As shown in Fig. 4(a), the $2^2\Sigma^+-1^4\Pi$, $2^2\Sigma^+-1^2\Pi$, $2^2\Sigma^+-2^4\Pi$, $2^2\Sigma^+-2^2\Pi$, and $2^2\Sigma^+-1^2\Sigma^-$ SOC integrals are in the range of 200–1000 cm^{-1}, indicating strong SOC between $2^2\Sigma^+$and $1^4\Pi$, $1^2\Pi$, $2^4\Pi$, $2^2\Pi$, as well as $1^2\Sigma^-$states. As shown in Fig. 4(b), in the region $R \geq 2.25$ Å, SOC integrals of the $2^2\Pi-1^4\Pi$, $2^2\Pi-1^4\Sigma^-$, and $2^2\Pi-1^2\Sigma^-$are monotonically increasing, while those of $2^2\Pi-1^4\Sigma^+$ and $2^2\Pi-1^4\Delta$ initially increase and then decrease as the internuclear distance increases. For large distances, $2^2\Pi-1^4\Pi$, $2^2\Pi-1^4\Sigma^-$and $2^2\Pi-1^2\Sigma^-$SOC integrals are much larger than the others, indicating the spin-orbit splitting of $2^2\Pi$ at dissociation limits are mainly caused by $1^4\Pi$, $1^4\Sigma^-$, and $1^2\Sigma^-$.

As shown in Fig. 1, the excited states $C^2\Pi$ and $B\ ^2\Sigma^+$ cross with each other at $R = 2.35$ Å, located at the vibrational level $\nu' = 0$ and 1 of the $2^2\Pi$ state. As shown in Fig. 4(a), the calculated SOC integral of $2^2\Sigma^+-2^2\Pi$ is about 280 cm^{-1} at the crossing point, which indicates a strong spin-orbit interaction and could be strong enough to introduce a predissociation pathway for $C(2)^2\Pi_{1/2}(\nu' \geq 1)$. This could be used to interpret the apparent perturbations between $B^2\Sigma^+{}_{1/2}$ and $C^2\Pi_{1/2}(\nu' \leq 2)$ found in the fluorescence excitation spectrum of the HgBr molecule [51].

3.4. Transition properties

The transition dipole moment (TDM) functions of $1^2\Pi$-$X^2\Sigma^+$, $C^2\Pi$-$X^2\Sigma^+$, and $B^2\Sigma^+$-$X^2\Sigma^+$are calculated and plotted in Fig. 5(a). In the Franck–Condon region, both TDMs of $C^2\Pi$-$X^2\Sigma^+$ and $B^2\Sigma^+$-$X^2\Sigma^+$are larger than that of $1^2\Pi$-$X^2\Sigma^+$. When considering the SOC, the TDMs curves from $1^2\Pi_{1/2}$, $1^2\Pi_{3/2}$, $C^2\Pi_{1/2}$, $D^2\Pi_{3/2}$, and $B^2\Sigma^+{}_{1/2}$ to $X^2\Sigma^+{}_{1/2}$ are displaced in Fig. 5(b). Comparing with $1^2\Pi$-$X^2\Sigma^+$, the $1^2\Pi_{3/2}$-$X^2\Sigma^+{}_{1/2}$ transition does not significantly change in the TDMs curves. However, $1^2\Pi_{1/2}$-$X^2\Sigma^+{}_{1/2}$ has somewhat changed, whose TDMs hold larger values than that of $1^2\Pi_{3/2}$-$X^2\Sigma^+{}_{1/2}$, especially in the large bond distance region. The crossing of $C^2\Pi$ and $B^2\Sigma^+$located at $R = 2.35$ Å leads to the exchange of wavefunctions for (3)1/2 and (4)1/2 states. Hence, for $R \geq 2.4$ Å,

Table 5
Radiative lifetimes of vibrational levels v'=0–5 of $C^2\Pi$, $B^2\Sigma^+$, $D^2\Pi_{3/2}$ and $B^2\Sigma^+_{1/2}$.

State	Radiative lifetimes (ns)					
	v'=0	v'=1	v'=2	v'=3	v'=4	v'=5
$C^2\Pi$	9.22	9.19	9.16	9.12	9.09	9.06
$B^2\Sigma^+$	19.29	19.09	18.89	18.70	18.51	18.32
$C^2\Pi_{1/2}$	11.24					
$D^2\Pi_{3/2}$	6.77	6.75	6.73	6.71	6.69	6.67
$B^2\Sigma^+_{1/2}$	21.75	21.13	20.89	20.66	20.44	20.22
Expt.[a]	23.7					
Expt.[b]	23.7 ± 1.5					
Calc.[c]	27.6					
Calc.[d]	16					

[a] Ref. [57].
[b] Ref. [55].
[c] Ref. [18].
[d] Ref. [58].

the TDMs of (3)1/2-$X^2\Sigma^+_{1/2}$ and (4)1/2-$X^2\Sigma^+_{1/2}$ originate from $B^2\Sigma^+_{1/2}$-$X^2\Sigma^+_{1/2}$ and $C^2\Pi_{1/2}$-$X^2\Sigma^+_{1/2}$, respectively.

The radiative lifetime of a vibrational level v' is given by the following formula [52–54] (1):

$$\tau = (A_{v'})^{-1} = \frac{3h}{64\pi^4 |a_0.e.TDM|^2 \sum_{v''} q_{v'v''} (\Delta E_{v'v''})^3} = \frac{4.936 \times 10^5}{|TDM|^2 \sum_{v''} q_{v'v''} (\Delta E_{v'v''})^3} \quad (1)$$

where *TDM* is in a.u., $q_{v'v''}$ are the Franck–Condon factors (FCFs) between the vibrational wave functions of v' and v'', energy gap $\Delta E_{v'v''}$ is in cm^{-1}, and radiative lifetime τ is in s.

Based on the calculated TDMs, FCFs, and energy gap ΔE, the radiative lifetimes of the low vibrational levels of $C^2\Pi$, $B^2\Sigma^+$, $C^2\Pi_{1/2}$, $D^2\Pi_{3/2}$, and $B^2\Sigma^+_{1/2}$ are calculated and listed in Table 5. The radiative lifetimes of these transitions are all in the order of 10 ns. Considering the SOC effect, the radiative lifetimes of $C^2\Pi_{1/2}$ and $D^2\Pi_{3/2}$ are slightly larger and smaller than that of $C^2\Pi$, respectively. Similarly, the radiative lifetimes of $B^2\Sigma^+_{1/2}$ are also slightly bigger than that of $B^2\Sigma^+$. The radiative lifetime of the vibrational level $v' = 0$ of $B^2\Sigma^+_{1/2}$ is calculated to be 21.75 ns, in good agreement with the previous experimental value 23.7 ± 1.5 ns [55].

4. Conclusions

High-level MRCI calculations on the PECs of 14 Λ-S states correlating to the asymptotes Hg(^{1}S) + Br(^{2}P) and Hg(^{3}P) + Br(^{2}P) of HgBr have been performed. For better accuracy, SOC and Davidson corrections are taken into consideration in our computations. The spectroscopic constants of the bound states are determined based on the PECs of the Λ-S and Ω states, which are in good agreement with the available experimental values. The SOC integral of $2^2\Sigma^+$–$2^2\Pi$ (280 cm^{-1}) at crossing point R = 2.35 Å indicates a strong spin-orbit interaction, which is consistent with the apparent perturbations between $B^2\Sigma^+_{1/2}$ and $C^2\Pi_{1/2}$ ($v' \leq 2$) found in the fluorescence excitation spectrum. The spin-excluded and spin-included TDMs of $1^2\Pi$-$X^2\Sigma^+$, $2^2\Pi$-$X^2\Sigma^+$, and $2^2\Sigma^+$-$X^2\Sigma^+$are calculated and the SOC influence on the TDMs is discussed. Based on the calculated TDMs, FCFs, and energy gap ΔE, the radiative lifetimes of the low vibrational levels of $C^2\Pi_{1/2}$, $D^2\Pi_{3/2}$ and $B^2\Sigma^+_{1/2}$ are calculated, where only the radiative lifetime of the vibrational level $v' = 0$ of $B^2\Sigma^+_{1/2}$ is experimentally reported. Our calculated value of the $v' = 0$ level of $B^2\Sigma^+_{1/2}$ is 21.75 ns, consistent with the experimental value 23.7 ± 1.5 ns. Our theoretical work reveals more helpful information on the spectroscopy of excited states for HgBr.

Declaration of Competing Interest

The authors declare that they have no known competing financial interests or personal relationships that could have appeared to influence the work reported in this paper.

CRediT authorship contribution statement

Shutao Zhao: Writing - original draft, Supervision. **Jicheng Cui:** Data curation. **Rui Li:** Visualization, Data curation. **Cunhua Zhang:** Software, Formal analysis. **Bing Yan:** Supervision, Writing - review & editing.

Acknowledgments

This work was supported by National Natural Science Foundation of China (Grant nos. 11604052, 11874177 and 11574114), the Natural Science Research Project of the Education Department of Anhui Province, China (Grant no. KJ2018A0342); the Excellent Youth Talent Project of the Education Department of Anhui Province, China (Grant no. gxyqZD2019046); the University Nursing Program for Young Scholars with Creative Talents in Heilongjiang Province, China (135409230); the key Program of Excellent Youth Talent Project of Fuyang Normal University, China (Grant no. rcxm201801); the Fuyang Municipal Government, Fuyang Normal University Horizontal Project (Grant no. XDHX201724) and the fund of the National Engineering Research Center for Diffraction Gratings Manufacturing and Application (Grant no. K201801).

Supplementary materials

Supplementary material associated with this article can be found, in the online version, at doi:10.1016/j.jqsrt.2020.107303.

References

[1] Küpper H, Andresen E. Mechanisms of metal toxicity in plants. Metallomics 2016.
[2] Ai S, Liu B, Yang Y, Ding J, Yang W, Bai X, et al. Temporal variations and spatial distributions of heavy metals in a wastewater-irrigated soil-eggplant system and associated influencing factors. Ecotox Environ Safe 2018;153:204–14.
[3] Shepler BC, Balabanov NB, Peterson KA. Ab Initio Thermochemistry Involving Heavy Atoms: an Investigation of the Reactions Hg + IX (X = I, Br, Cl, O). Phys Chem A 2005;109:10363–72.
[4] Shepler BC, Balabanov NB, Peterson KA. Hg+Br→HgBr recombination and collision-induced dissociation dynamics. J Chem Phys 2007;127:164304.
[5] Schimitschek EJ, Celto JE, Trias JA. Mercuric bromide photodissociation laser. Appl Phys Lett 1977;31:608–10.
[6] Schimitschek EJ, Celto JE. Mercuric bromide dissociation laser in an electric discharge. Opt Lett 1978;2:64–6.
[7] Kushawaha V, Michael A, Mahmood M. Collision-induced dissociative processes relevant to mercury halide lasers. J Phys B 1988;21:2507.
[8] Prasannaa VS, Vutha AC, Abe M, Das BP. Mercury monohalides: suitability for electron electric dipole moment searches. Phys Rev Lett 2015;114:183001.
[9] Wieland K. Bandenspektren der quecksilber-, cadmium- und zinkhalogenide. Helv Phys Acta 1929;2:46.
[10] Sastry M. The ultra-violet band spectrum of mercury bromide. Proc Natl Inst Sci India 1941;7:359.
[11] Howell HG. The ultra-violet spectra and electron configuration of HgF and related halide molecules. Proc R Soc Lond A 1943;182:95–112.
[12] Rao K, Rao G. A new band system of the HgBr molecule. Indian J Phys 1944;18:281.
[13] Krishnamurthy VG. Ultraviolet bands of mercury bromide. Z Phys 1958;152:242–8.
[14] Greig G. Reactions of metal atoms. II. The combination of mercury and bromine atoms and the dimerization of HgBr. J Chem Phys 1970;52:3684.
[15] Misra P, Michael A, Kushawaha V. Emission studies involving the formation of (C-X) and (D-X) band systems of HgX (X=Cl,Br,I) radicals. Spectrosc Lett 1991;24:847–54.
[16] Mazza C. Laser induced fluorescence measurement of HgBr (B→X) radiative lifetime. Chem Phys Lett 1977;46:172–4.
[17] Tellinghuisen J, Ashmore JG. The B→X transition in $^{200}Hg^{79}Br$. Appl Phys Lett 1982;40:867–9.
[18] Wadt WR. The electronic structure of HgCl and HgBr. Appl Phys Lett 1979;34:658–60.

[19] Bhartiya JB, Behere SH, Rao MLP. Dissociation energies of HgCl, HgBr and HgI from potential energy curves. J Quant Spectrosc Radiat Transfer 1990;43:95–8.
[20] Liao M, Zhang Q, Schwarz WHE. Properties and Stabilities of MX, MX_2, and M_2X_2 Compounds (M = Zn, Cd, Hg; X = F, Cl, Br, I). Inorg Chem 1995;34:5597–605.
[21] Li R, Zhang H, Liu X, Zhao S, Liu Y, Yan B. Electronic structures and spectroscopic properties of CdI: MRCI+Q study including spin-orbit coupling. J Quant Spectrosc Radiat Transf 2018;205:71–9.
[22] Yuan X, Yin S, Shen Y, Liu Y, Lian Y, Xu H-F, et al. Laser cooling of thallium chloride: a theoretical investigation. J Chem Phys 2018;149:094306.
[23] Werner H.-J., Knowles P.J., Knizia G., Manby F.R., Schütz M., Celani P., et al. MOLPRO, version 2010.1, a package of ab initio programs; 2010.
[24] Peterson KA, Puzzarini C. Systematically convergent basis sets for transition metals. II. Pseudopotential-based correlation consistent basis sets for the group 11 (Cu, Ag, Au) and 12 (Zn, Cd, Hg) elements. Theor Chem Acc 2005;114:283–96.
[25] Figgen D, Rauhut G, Dolg M, Stoll H. Energy-consistent pseudopotentials for group 11 and 12 atoms: adjustment to multi-configuration Dirac–Hartree–Fock data. Chem Phys 2005;311:227–44.
[26] Peterson KA, Yousaf KE. Molecular core-valence correlation effects involving the post-d elements Ga–Rn: benchmarks and new pseudopotential-based correlation consistent basis sets. J Chem Phys 2010;133:174116.
[27] Peterson KA, Figgen D, Goll E, Stoll H, Dolg M. Systematically convergent basis sets with relativistic pseudopotentials. II. Small-core pseudopotentials and correlation consistent basis sets for the post-d group 16–18 elements. J Chem Phys 2003;119:11113.
[28] Knowles PJ, Werner H-J. An efficient second-order MC SCF method for long configuration expansions. Chem Phys Lett 1985;115:259–67.
[29] Werner H-J, Knowles PJ. A second order multiconfiguration SCF procedure with optimum convergence. J Chem Phys 1985;82:5053–63.
[30] Knowles PJ, Werner H-J. An efficient method for the evaluation of coupling coefficients in configuration interaction calculations. Chem Phys Lett 1988;145:514–22.
[31] Werner H-J, Knowles PJ. An efficient internally contracted multiconfiguration–reference configuration interaction method. J Chem Phys 1988;89:5803–14.
[32] Tilson JL, Ermler WC. Massively parallel spin–orbit configuration interaction. Theor Chem Acc 2014:133.
[33] Berning A, Schweizer M, Werner H-J, Knowles PJ, Palmieri P. Spin-orbit matrix elements for internally contracted multireference configuration interaction wavefunctions. Mol Phys 2000;98:1823–33.
[34] Pitzer RM, Winter NW. Electronic-structure methods for heavy-atom molecules. J Phys Chem 1988;92:3061–3.
[35] Le Roy R. LEVEL8.0: a computer program for solving the radial Schrödinger equation for bound and quasibound levels. Chemical physics research report CP-663. University of Waterloo; 2007.
[36] Moore CE. Atomic energy levels. Washington(DC): National Bureau of Standards; 1971.
[37] Wieland K. Bandensysteme B $(^2\Sigma^+)\rightarrow X\ (^2\Sigma^+)$ und Dissoziationswerte der Radikale HgJ und HgBr. Zeitschrift Für Elektrochemie, Berichte Der Bunsengesellschaft Für Physikalische Chemie 1960;64:761–9.
[38] Li R, Wang M, Zhao S, Zu N, Yan B. Spin-orbit calculations on the ground and excited electronic states of CdBr molecule. J Quant Spectrosc Radiat Transf 2018;221:110–17.
[39] Balasubramanian K. Spectroscopic constants and potential-energy curves of heavy p-block dimers and trimers. Chem Rev 1990;90:93–167.
[40] Alekseyev AB, Liebermann H-P, Buenker RJ. Spin-orbit multireference configuration interaction method and applications to systems containing heavy atoms. In: Recent advances in relativistic molecular theory. Singapore: World Scientific; 2004. p. 65–105.
[41] Minaev BF, Knuts S, Ågren H. On the interpretation of the external heavy atom effect on singlet-triplet transitions. Chem Phys 1994;181:15–28.
[42] Minaev B. Ab initio study of low-lying triplet states of the lithium dimer. Spectrochim Acta A 2005;62:790–9.
[43] Minaev B, Yaschuk L, Kukueva V. Calculation of the fine structure and intensity of the singlet–triplet transitions in the imidogen radical. Spectrochim Acta A 2005;61:1105–12.
[44] DeYonker NJ, Allen WD. Taming the low-lying electronic states of FeH. J Chem Phys 2012;137:234303.
[45] Liu S, Zhang X, Zhai H, Liu Y. Accurate predictions of spectroscopic and molecular properties of the NTe molecule. J Quant Spectrosc Radiat Transf 2017;202:50–7.
[46] Linn SH, Tzeng W-B, Brom JM, Ng CY. Molecular beam photoionization study of $HgBr_2$ and HgI_2. J Chem Phys 1983;78:50–61.
[47] Huber KP, Herzberg G. Molecular spectra and molecular structure: IV. Constants of diatomic molecules. New York: Van Nostrand Reinhold; 1979.
[48] Tellinghuisen J, Ashmore JG. Mixed representations for diatomic spectroscopic data: application to HgBr. Chem Phys Lett 1983;102:10–16.
[49] Rai AK, Rai SB, Rai DK. Ultraviolet bands in diatomic mercury bromide. J Phys B 1983;16:1907.
[50] Papagiannakopoulos P, Zevgolis D. Laser emission at 502nm induced by KrF laser multiphoton dissociation of $HgBr_2$. In: Advances in chemical reaction dynamics. Dordrecht: Springer; 1986. p. 475–82.
[51] Lipson RH, Jordan KJ, Bascal HA. Fluorescence excitation spectra of jet-cooled HgBr radicals. J Chem Phys 1993;98:959–67.
[52] Okabe H. Photochemistry of small molecules. New York: Wiley; 1978.
[53] Heaven MC. Fluorescence decay dynamics of the halogens and interhalogens. Chem Soc Rev 1986;15:405.
[54] Liu K, Yu L, Bian W. Extensive theoretical study on various low-lying electronic states of silicon monochloride cation including spin–orbit coupling. J Phys Chem A 2009;113:1678–85.
[55] Waynant RW, Eden JG. HgX (B) radiative lifetime by fast photolysis of HgX_2 (X=Br,I). Appl Phys Lett 1978;33:708–10.
[56] Gerhard Herzberg. Molecular spectra and molecular structure. I. Spectra of diatomic molecules. New York: Van Nostrand Reinhold; 1950.
[57] Roxlo C, Mandl A. Quenching kinetics for the HgBr* $(B^2\Sigma_{1/2})$ and HgI* $(B^2\Sigma_{1/2}, C^2\Pi_{1/2})$ states. J Chem Phys 1980;72:541–3.
[58] Duzy C, Hyman HA. Radiative lifetimes for the B→X transition in HgCl, HgBr, and HgI. Chem Phys Lett 1977;52:345–8.